Antiviral Research 101 (2014) 82–92

Contents lists available at ScienceDirect

Antiviral Research

journal homepage: www.elsevier.com/locate/antiviral

A 3C^{pro}-dependent bioluminescence imaging assay for *in vivo* evaluation of anti-enterovirus 71 agents

Zhiwei Guo [a], Xiaoyan Zhong [a], Lexun Lin [a], Shuo Wu [a], Tianying Wang [a], Yang Chen [a], Xia Zhai [a], Yan Wang [a], Heng Wu [a], Lei Tong [a], Yelu Han [a], Bo Pan [a], Yihong Peng [c], Xiaoning Si [a], Fengmin Zhang [a], Wenran Zhao [b,*], Zhaohua Zhong [a,*]

[a] Department of Microbiology, Harbin Medical University, Harbin 150081, China
[b] Department of Cell Biology, Harbin Medical University, Harbin 150081, China
[c] Department of Microbiology, Peking University Health Science Center, Beijing 100191, China

ARTICLE INFO

Article history:
Received 8 July 2013
Revised 1 November 2013
Accepted 6 November 2013
Available online 18 November 2013

Keywords:
Enterovirus 71
Split luciferase
3C protease
In vivo imaging

ABSTRACT

Enterovirus 71 (EV71), a member of *Picornaviridae*, is one of the major pathogens of human hand, foot and mouth disease. EV71 mainly infects children and causes severe neurological complications and even death. The pathogenesis of EV71 infection is largely unknown, and no clinically approved vaccine or effective treatment is available to date. Here we described a novel bioluminescence imaging approach for EV71 detection. In this approach, a plasmid-based reporter was constructed to express the fusion protein AmN(Q/G)BC, a split firefly luciferase mutant, which can be specifically cleaved by EV71 protease 3C^{pro}. Upon cleavage, the splitting fusion protein restores luciferase activity. Our test confirmed that AmN(Q/G)BC was specifically cleaved by 3C^{pro} and EV71 and restored the luciferase activity to a degree that corresponds to the 3C^{pro} and virus doses in cells and mice. The anti-EV71 effect of GW5074 and U0126, two mitogen-activated protein kinase (MAPK) inhibitors, was evaluated using this approach to validate its application of screening anti-EV71 agents. We found that the AmN(Q/G)BC reporter efficiently monitored the inhibitory effect of GW5074 and U0126 on EV71 infection under *in vitro* and *in vivo* conditions. The data from AmN(Q/G)BC reporter were consistent with Western blotting and histopathology examination. Taken together, this real-time imaging approach can quantitatively monitor the efficacy of anti-EV71 agents and is valuable for anti-EV71 drug screening and evaluation, especially, under *in vivo* conditions.

1. Introduction

Enterovirus 71 (EV71) belongs to the enterovirus genus of the *Picornaviridae* family. It is the major pathogen of human hand, foot, and mouth disease (HFMD) (Li et al., 2012a; Zeng et al., 2012a). HFMD is a common illness in the Asia–Pacific region, and outbreaks occur periodically (Li et al., 2012a; Zeng et al., 2012a). Although EV71 infection causes mild symptoms in most cases, it leads to severe consequences and even death in some patients especially in children under 5 years old. EV71-caused cerebral infection and pulmonary edema are fatal (Xu et al., 2012). There is no currently available specific chemotherapy and vaccine against EV71 infection (Chang et al., 2012; Li et al., 2012b; Xu et al., 2010; Zhu et al., 2013). There is an urgent need for an effective anti-EV71 agent for the control of EV71 infection.

EV71 infection can be detected by reverse transcription-polymerase chain reaction (RT-PCR), real-time PCR, Western blotting, plaque forming, etc. Bioluminescence imaging has been increasingly used to study cancer, microbial infection, and viral pathogenesis (Au et al., 2012; Brock, 2012; Du et al., 2010; Madero-Visbal et al., 2012; Snoeks et al., 2012; Wang et al., 2010). *In vivo* imaging assays are especially useful for quantitative and real-time-based detection of viral infection (Heaton et al., 2013; Sewald et al., 2012) and can therefore greatly simplify and speed antiviral agent screening from libraries of existing or synthesized chemical compounds. To date, a specific *in vivo* imaging assay for picornaviruses, including EV71, is not available.

Neonatal ICR and Balb/c mice have been successfully used for evaluating the neuropathogenesis and immunization of EV71 (Chen et al., 2004; Yu et al., 2000; Khong et al., 2011). To establish an *in vivo* imaging assay for the detection of picornavirus infection, we tried to develop a replication-competent fluorescence protein- or luciferase-expressing picornavirus variant by integrating the reporter gene into the full-length viral genome. Using this strategy,

* Corresponding authors. Tel./fax: +86 451 86685122 (Z. Zhong). Tel.: +86 451 86612713 (W. Zhao).
E-mail addresses: zhaowr@ems.hrbmu.edu.cn (W. Zhao), zhongzh@hrbmu.edu.cn (Z. Zhong).

0166-3542/$ - see front matter © 2013 Elsevier B.V. All rights reserved.
http://dx.doi.org/10.1016/j.antiviral.2013.11.002

enhanced green fluorescence protein (EGFP)-, mCherry-, and *Renilla* luciferase (RLuc)-tagged coxsackievirus B3 variants (Tong et al., 2011; Wang et al., 2012c) were established. These variants are extremely convenient to visually monitor virus infection *in vitro*. However, there are critical defects within these variants. The engineered viral genome is usually destabilized because of the reporter gene integration (Lee et al., 2002; Tong et al., 2011; Wang et al., 2012c). The engineered virus phenotype may not be quite the same as the wild-type (Geiss et al., 2011; Shang et al., 2012a). Hence, the data from the engineered virus need extra verification based on the wild-type strain. Furthermore, EGFP and RLuc emit green and blue light that is not well transmitted through tissues (Doyle et al., 2004). These shortcomings make it difficult to monitor the virus infection *in vivo*.

Firefly (*Photinus pyralis*) luciferase (Luc) produces red light emission (565 nm), which is well transmitted through tissues and is therefore the preferred luciferase for *in vivo* bioluminescence imaging (Doyle et al., 2004). To facilitate monitoring EV71 infection *in vivo*, we first tried to develop a Luc-expressing EV71 variant using the aforementioned strategy but were not successful. The possible reason is that the 1.6 kb Luc-coding sequence is too large and is beyond the maximal viral capacity for an exogenous gene (10%). The attempt to construct a Luc-expressing coxsackievirus B3 also failed (Lim et al., 2005b).

A split luciferase bioluminescence assay has been developed to measure protein interactions, phosphorylation, and enzyme cleavage of substrates (Shekhawat and Ghosh, 2011). Luciferase can be enzymatically deactivated by inserting a target peptide between its N and C fragments. Upon cleaving the target peptide, the fragments may be able to reconstitute enzymatic activity and generate luminescence in cells and animals (Shekhawat and Ghosh, 2011). EV71 encodes two proteases $2A^{pro}$ and $3C^{pro}$, which cleave the viral polyprotein into the structural capsid proteins and nonstructural proteins (Shih et al., 2011). $3C^{pro}$ plays a vital role in EV71 replication because the majority of the viral nonstructural proteins are released by the cleavage of $3C^{pro}$ or its precursor 3CD (Cui et al., 2011; Lu et al., 2011; Shih et al., 2011; Zhang et al., 2013). $3C^{pro}$ recognizes and cleaves proteins with glutamine (Q)-glycine (G) bonds, especially the AxxQ/G sequence [A: alanine; x: any amino acid (aa), the slash represents the cleavage site] (Nicklin et al., 1988; Weng et al., 2009). Therefore, the split luciferase bioluminescence strategy may be applicable for EV71 detection.

Screening chemical compound libraries, traditional medicines, and small interfering RNAs (siRNAs) leads to the discovery of some potential anti-EV71 agents (Arita et al., 2008; Deng et al., 2012; Pourianfar et al., 2012; Shang et al., 2012b; Tan et al., 2007; Wang et al., 2012b; Wu et al., 2009; Yang et al., 2012a,b; Zhang et al., 2013). GW5074 and U0126 have recently been shown to be able to suppress EV71 replication *in vitro* (Arita et al., 2008, 2009; Wang et al., 2012a). GW5074 is a benzylidine oxindole derivative and a selective Raf-1 inhibitor (Bain et al., 2007; Chen et al., 2008). U0126 inhibits the phosphorylation of MEK1 and MEK2 (MEK1/2). Both Raf-1 and MEK1/2 are essential components in the activation cascades of the mitogen-activated protein kinase (MAPK) pathway (Johnson and Lapadat, 2002).

In this study, we adapted the split luciferase bioluminescence strategy to generate an AmN(Q/G)BC reporter for monitoring EV71 infection through response to the presence of EV71 $3C^{pro}$. Experimental therapy for EV71 cerebral infection with GW5074 and U0126 were used to validate its value in the *in vivo* application for EV71 infection. Our data show that this approach could quantitatively trace EV71 infection in real-time manner. The anti-EV71 effect of GW5074 and U0126 was efficiently evaluated using this approach. This novel bioluminescence imaging assay may be valuable for fast screening and evaluation of anti-EV71 agents.

2. Materials and methods

2.1. Cells and virus

Vero (African green monkey kidney) cells were maintained and passaged in Dulbecco's modified Eagle's medium (DMEM) supplemented with 5% fetal bovine serum (FBS) (Biological Industries, Israel), 100 μg/ml penicillin, and 100 μg/ml streptomycin at 37 °C with 5% CO_2 in a humidified incubator. After virus inoculation, the cells were maintained in DMEM with 2% FBS or without FBS. The EV71 BrCr strain was a kind gift from Professor Mingli Wang, Department of Microbiology, Anhui Medical University, Hefei, China. The viruses were passaged in Vero cells and titrated using the 50% tissue culture infective dose (TCID50) assay (Liu et al., 2007). Briefly, Vero cells were seeded in 96-well plates at 1×10^4 cells/well and cultured overnight. Serial diluted viruses were inoculated into the cells (10 wells for each dilution). The cells were incubated at 37 °C with 5% CO_2 for 3 days and stained with 0.4% trypan blue solution. TCID50 was calculated using the method described by Reed and Muench (Krah, 1991).

2.2. Chemicals

GW5074 [3-(3,5-Dibromo-4-hydroxybenzyliden)-5-iodo-1,3-dihydroindol-2-one] and U0126 [1,4-Diamino-2,3-dicyano-1,4-bis(o-aminophenylmercapto)butadiene] were purchased from Sigma (St. Louis, MO). GW5074 or U0126 was dissolved in DMSO at 10 mM and stored at -20 °C.

2.3. Plasmid construction and site-directed mutagenesis

A reporter plasmid pAN(Q/G)BC was constructed based on pcDNA3.1(+) (Promega, Madison, WI) to express polyprotein AN(Q/G)BC. AN(Q/G)BC is a split Luc with three insertions, including oligopeptide AVMQGASIQG, peptide A (pepA), and peptide B (pepB). To maintain the flexibility of the fusion protein, a linker oligopeptide was added to the pepA - N and pepB – C links, respectively (Table S1). A triglycine linker was added to both ends of oligopeptide AVMQGASIQG (Table S1). To trace the plasmid expression, an EGFP expression cassette was added downstream to the AN(Q/G)BC cassette (Fig. 1A). The N and C fragments were obtained by PCR from pGL4.17 (Promega). The EGFP-coding sequence was obtained by PCR from pEGFP-N1 (Clontech, Mountain View, CA).

There are two Q–G bonds in the prototype Luc (Q159–G160 and Q338–G339 in the N fragment), which may be cleaved by EV71 $3C^{pro}$. To discard the $3C^{pro}$ Cleavage to Luc itself, the Q–G bonds were removed by site-directed mutations of Q159M and Q338C with overlapping PCR. The AN(Q/G)BC derived from the mutated N fragment was designated as AmN(Q/G)BC.

A plasmid expressing EV71 $3C^{pro}$ fused with EGFP was generated based on pEGFP-C1 (Wang et al., 2012c) and designated as pEGFP-3C. The $3C^{pro}$ sequence was obtained from the EV71 BrCr strain by RT-PCR. An attenuated $3C^{pro}$ mutant (m3C) was also prepared with the substitution of C147S (Weng et al., 2009) in pEGFP-3C, and the resultant plasmid was designated as pEGFP-m3C (Fig. 2E). The primers (Table S2) were synthesized by GenePharma (Shanghai, China). To introduce these plasmids into cells, Lipofectamine 2000 reagent (Invitrogen, Carlsbad, CA) was used according to the manufacturer's protocol.

2.4. Cell viability

Cell viability was assessed by MTT (thiazolyl blue tetrazolium bromide) (Invitrogen) assay. Briefly, Vero cells were seeded in

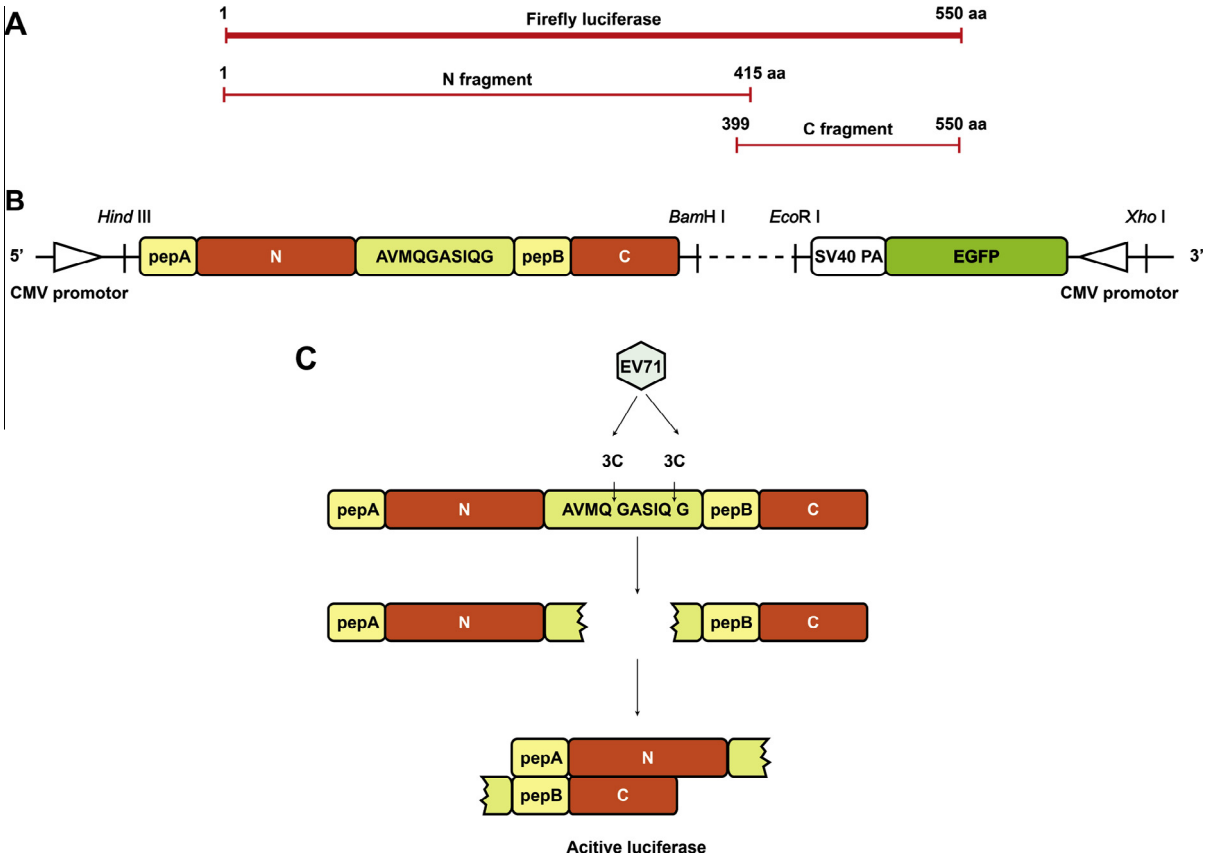

Fig. 1. The design of the EV71 $3C^{pro}$-dependent split luciferase imaging reporter. (A) The N and C fragments of Luc. (B) There are two expression cassettes in the reporter plasmid: the AN(Q/G)BC-expressing cassette and the EGFP-expressing cassette. In the AN(Q/G)BC-expressing cassette, the Luc was split into N and C fragments by the oligopeptide AVMQGASIQG, which contains two EV71 $3C^{pro}$ cleavage sites. The N and C fragments were fused with pepA and pepB at the N-terminals. (C) Upon the cleavage of $3C^{pro}$, the N fragment links to the C fragment through the intrinsic interaction of pepA and papB. Consequently, the Luc activity is restored.

96-well plates at 1×10^4 cells/well and cultured overnight. The cells were inoculated with EV71 (1.5×10^6 TCID50) and simultaneously administered GW5074, U0126, and GW5074 + U0126 at various concentrations. The cell viability was examined at an interval of 6 h from 0 to 24 h post-infection (p.i.). Approximately 20 μl of 5 mg/ml MTT was added to the cells after the culture medium was removed. The MTT solution was discarded 4 h later, and 150 μl of dimethyl sulfoxide (DMSO) was added, and vigorous shaking for 10 min was performed. The optical absorption was read by a colorimetric reader at 490 nm. The cell viability was plotted with the percentage of absorbance compared to the untreated cells (NC) at each time point.

2.5. RT-PCR

Total RNA was extracted with TRIzol reagent (Invitrogen) according to the manufacturer's instructions. RT-PCR was performed with PrimeScript RT reagent kit (TaKaRa, Ohtsu, Shiga, Japan) and β-actin was used as the internal control. The primers for $3C^{pro}$ and β-actin mRNA are listed in Table S2. PCR products were analyzed using 1% agarose gel electrophoresis.

2.6. Western blotting

Proteins were extracted from cell lysates using Pierce RIPA Buffer with PMSF protease inhibitor cocktail (Thermo, Rockford, IL), and applied to sodium dodecyl sulfate–polyacrylamide gel electrophoresis (SDS–PAGE). The separated proteins were electro-transferred to polyvinylidene fluoride (PVDF) film (0.45 μm, Millipore, Billarica, MA) and incubated with primary antibody at 4 °C overnight. After routine washing, the film was incubated with horseradish peroxidase (HRP)-labeled antibody at room temperature for 1 h. The blots were stained with a Pierce ECL Plus kit (Thermo) and imaged with a charge-coupled camera LAS4000 (Fujifilm, Tokyo, Japan). The primary antibodies used in this study included antibodies against Luc (Millipore, diluted at 1:10, 000), ERK1/2, p-ERK1/2, Raf-1 (Cell Signaling, Boston, MA, diluted at 1:1000), p-Raf-1, β-actin (Santa Cruz Biotechnology, Santa Cruz, CA, diluted at 1:1000), and enterovirus VP1 (Clone 5-D8/1) (Dako, Glostrup, Denmark, diluted at 1:1000).

2.7. In vitro bioluminescence assay

The total photonic fluxes of cells cultured in 6-well or 24-well plates were measured using a charge-coupled camera IVIS Lumina (Xenogen, Hopkinton, MA). Before the measurement, the medium was replaced by DMEM with 5% FBS and 50 μg/ml D-luciferin (Cellcyto, Beijing, China). After incubation at 37 °C for 10 min, the photonic emission was photographed by IVIS Lumina at 565 nm for approximately 1 min (with a 15 cm field of view, binning factor of 8, 1/*f* stop, open filter). The total flux was quantified as the sum of all detected photon counts (photons/s/cm^2) within the region of interest (ROI) using the Living Image 3.1 software (Xenogen).

2.8. Cerebral infection and in vivo bioluminescence assay

Specific-pathogen-free (SPF) suckling ICR mice were obtained from Vital River Laboratories (Beijing, China) and maintained in standard conditions (12 h bright/12 h dark with free access to food

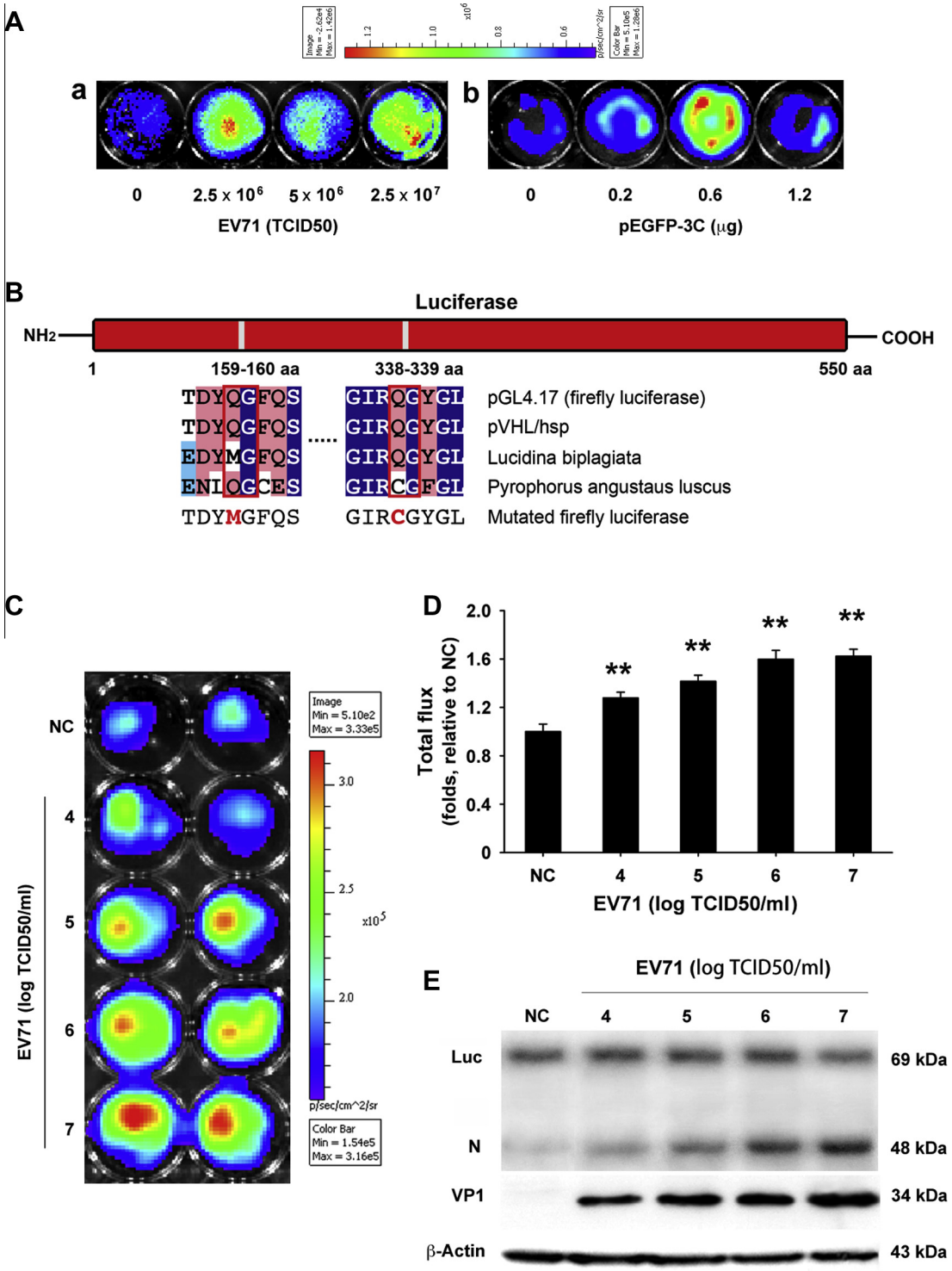

Fig. 2. The mutations that disrupt the potential $3C^{pro}$ cleavage to the N fragment of the AN(Q/G)BC reporter lead to the linear relationship between the Luc activity restoration and the viral doses. (A) The total photonic fluxes in the pAN(Q/G)BC-transfected cells with EV71 infection or pEGFP-3C transfection was not viral dose- or plasmid dose-dependent. (a) Vero cells in 24-well plates were transfected with pAN(Q/G)BC. The cells were infected with EV71 (0, 2.5×10^6, 5×10^6, 2.5×10^7 TCID50, respectively). The bioluminescence imaging was performed at 4 h p.i. with an IVIS Lumina camera. (b) Vero cells in 24-well plates were transfected with pAN(Q/G)BC for 24 h and then transfected with pEGFP-3C (0, 0.2, 0.6, and 1.2 μg, respectively). The bioluminescence imaging was performed at 24 h after the second transfection. (B) The mutations that remove the potential $3C^{pro}$ cleavage to the Luc itself. There are two Q–G bonds in the Luc molecule (Q159–G160, Q338–G339) that may be cleaved by $3C^{pro}$. Based on the sequence alignment of various luciferase species, Q159M and Q338C mutations were performed to eliminate the potential $3C^{pro}$ cleavage yet reserve the Luc activity. The mutated AN(Q/G)BC was designated as AmN(Q/G)BC. (C–E) The Luc activity in the EV71-infected Vero cells with pAmN(Q/G)BC. Vero cells in 24-well plates were transfected with pAmN(Q/G)BC. The cells were infected with serially diluted EV71 (in 500 μl) at 24 h post-transfection. The bioluminescence was detected at 4 h p.i. (C). The total flux of the infected cells was normalized by that of the NC group. Error bars represent SE ($n = 3$). ** stands for $P < 0.01$ compared with NC (D). The protein expression of Luc, N fragment, and VP1 as detected by western blotting at 7 h p.i. (E).

and water) in the Laboratory Animal Center of Harbin Medical University. The animal experiments were approved by the Experimental Ethics Committee of Harbin Medical University and performed according to the Guidelines of Laboratory Animal Usage of Harbin Medical University that is basically in accordant with the Guideline of Institutional Animal Care and Use Committee, USA.

The ICR mice (3-day-old) were anesthetized and manually restrained on the bench. Approximately 2×10^7 TCID50 of EV71 in 20 μl was inoculated using a 27G needle after it had directly penetrated the cranium (Shimizu, 2004). The infected mice were peritoneally administered GW5074 (0.2 mg/kg), U0126 (2.0 mg/kg), and GW5074 + U0126 (0.2 + 2.0 mg/kg), respectively, on day 1, 3, and 5 p.i. Meanwhile, each mouse was administered 10 μg of pAmN(Q/G)BC by intracerebral injection. Non-infected mice treated with the drugs served as the controls (NC). The sham mice (Sham) were inoculated with viruses and plasmids but were not administered drugs. The bioluminescence in the mouse brain was examined on day 2, 4, and 6 p.i. Before image acquisition, the mice were anesthetized with an intraperitoneal injection of 4 % chloral hydrate at a dose of 0.5 ml per 100 g of body weight. Once anesthetized, each mouse received intracerebral injections with 10 μl of D-luciferin (3 mg/ml) in PBS. Photons emitted from the mouse brain were recorded by IVIS Lumina and presented as a pseudocolor image overlaid on the gray-scale body image. The average acquisition time for the luminescence image was 1 min.

2.9. Histopathology examination

The suckling ICR mice with various treatments were sacrificed on day 6 post-treatment, and the brain, heart, kidney, liver, and lung were carefully excised from the mice. The tissues were washed in cold PBS and then fixed in 4% neutral formalin for 24 h. The fixed tissues were then embedded in paraffin, sectioned at a thickness of 5 μm and stained with hematoxylin and eosin (HE).

2.10. Statistical analysis

The data are presented as the mean ± standard deviation (SD) or the mean ± standard error (SE). Student's *t*-test was used for the statistical analysis by SigmaStat 3.1 (Systat Software, Richmond, CA). All experiments were repeated at least three times.

3. Results

3.1. AN(Q/G)BC can be specifically cleaved by EV71 $3C^{pro}$

To monitor EV71 infection, we designed a polyprotein AN(Q/G)BC (Fig. 1B). The polyprotein is a split Luc with an oligopeptide AVMQGASIQG insertion. The oligopeptide contains two EV71 $3C^{pro}$ cleavage sites (AxxQ/G). Two fragments of Luc, N-fragment (N, 1–415 aa) and C-fragment (C, 399–550 aa) (Fig. 1A), were fused with pepA and pepB at the N-terminals, respectively. PepA and pepB can link together intrinsically with high affinity (Sewald et al., 2012; Thormeyer et al., 2003). The intervening oligopeptide blocks the interaction of pepA and papB. The splitting deactivates the Luc enzymatic activity. If there were EV71 or $3C^{pro}$ present, the oligopeptide cleavage would allow pepA to link to pepB, which would bring the N fragment in close proximity to the C fragment. As a result, the Luc activity is restored (Fig. 1B).

In the Vero cells transfected with pAN(Q/G)BC, EGFP was expressed in cells 24 h post-transfection (data not shown). Sequencing confirmed that the AN(Q/G)BC-coding sequence was exactly as our design.

To verify the specific cleavage of $3C^{pro}$, Vero cells were transfected with pAN(Q/G)BC and cultured for 24 h. The cells were then transfected with pEGFP-3C and pEGFP-m3C and cultured for another 24 h. RT-PCR with $3C^{pro}$-specific primers showed that either $3C^{pro}$ or m3C was expressed in the transfected cells (Fig. S1D). The Luc activity of the cells transfected with pEGFP-3C was increased significantly compared with that of the cells with pEGFP-C1 ($P < 0.01$) (Fig. S1A and S1B). There was no significant difference between the photonic fluxes of the cells with pEGFP-m3C and pEGFP-C1 ($P > 0.05$) (Fig. S1A and S1B). Western blotting showed the N fragment in the cells with pEGFP-3C but not in the cells with pEGFP-C1 and pEGFP-m3C (Fig. S1C). These data indicate that AN(Q/G)BC could be specifically cleaved by $3C^{pro}$.

3.2. The Luc activity restoration of AN(Q/G)BC does not correspond with the virus or $3C^{pro}$ dose

Vero cells transfected with pAN(Q/G)BC were infected with various doses of EV71 at 24 h post-transfection. The Luc bioluminescence was detected at 4–24 h p.i. Surprisingly, we found that the Luc activity restoration in the cells did not increase according to the viral doses (Fig. 2A). We repeated this detection with pEGFP-3C instead of EV71. The Luc restoration was not consistent with the dose of pEGFP-3C either (Fig. 2A).

The inconsistency between the Luc restoration and viral dose suggested that the Luc itself might be deactivated by $3C^{pro}$. Indeed, two Q–G bonds were identified in the N fragment (Q159–G160 and Q338–G339) (Fig. 2B). The sequence alignment of the various luciferase species suggested that the substitutions of Q159M and Q338C preserves the Luc activity (Fig. 2B). Thus, the N fragment was site-directed mutated with Q159M and Q338C substitutions to eliminate the potential $3C^{pro}$ cleavage sites. The polypeptide AN(Q/G)BC with the mutations was designated as AmN(Q/G)BC.

3.3. EV71 infection can be quantitatively detected by AmN(Q/G)BC in vitro

Vero cells were then transfected with pAmN(Q/G)BC for 24 h and infected with various doses of EV71. The photonic fluxes were measured at 4 h p.i., and the N fragment and EV71 capsid protein VP1 were detected at 7 h p.i. The VP1 levels increased according to the viral inoculation (Fig. 2E). The total flux in the infected cells increased corresponding to the inoculated virus doses ($P < 0.01$, compared with NC) (Fig. 2C and D). The N protein level was also accordingly increased in the infected cells in a dose-dependent manner (Fig. 2E). The Luc restoration was parallel to the EV71 dose.

3.4. EV71 cerebral infection can be visually traced by AmN(Q/G)BC

Three-day-old ICR mice were intracerebrally inoculated with 2×10^7 TCID50 of EV71. pAmN(Q/G)BC (10 μg/mouse) was administered to the mice in the same way 24 h before bioluminescence detection. All mice with plasmid inoculation were EGFP fluorescence positive (509 nm) in the inoculated location on day 2 and 6 p.i. (Fig. S2). Compared with the sham group, the total fluxes of the infected mice was approximately 5, 8, and 16-fold higher on day 2, 4, and 6 p.i., respectively (Fig. 3A and B). The N and VP1 proteins were also expressed in the infected brain tissues (Fig. 3C). The infected mice developed severe weight loss, hind limb paralysis (Fig. 3D, arrow; Video S2), and skin lesions from day 4 to day 6 p.i. Taken together, this reporter could visually measure the EV71 cerebral infection in a real-time manner.

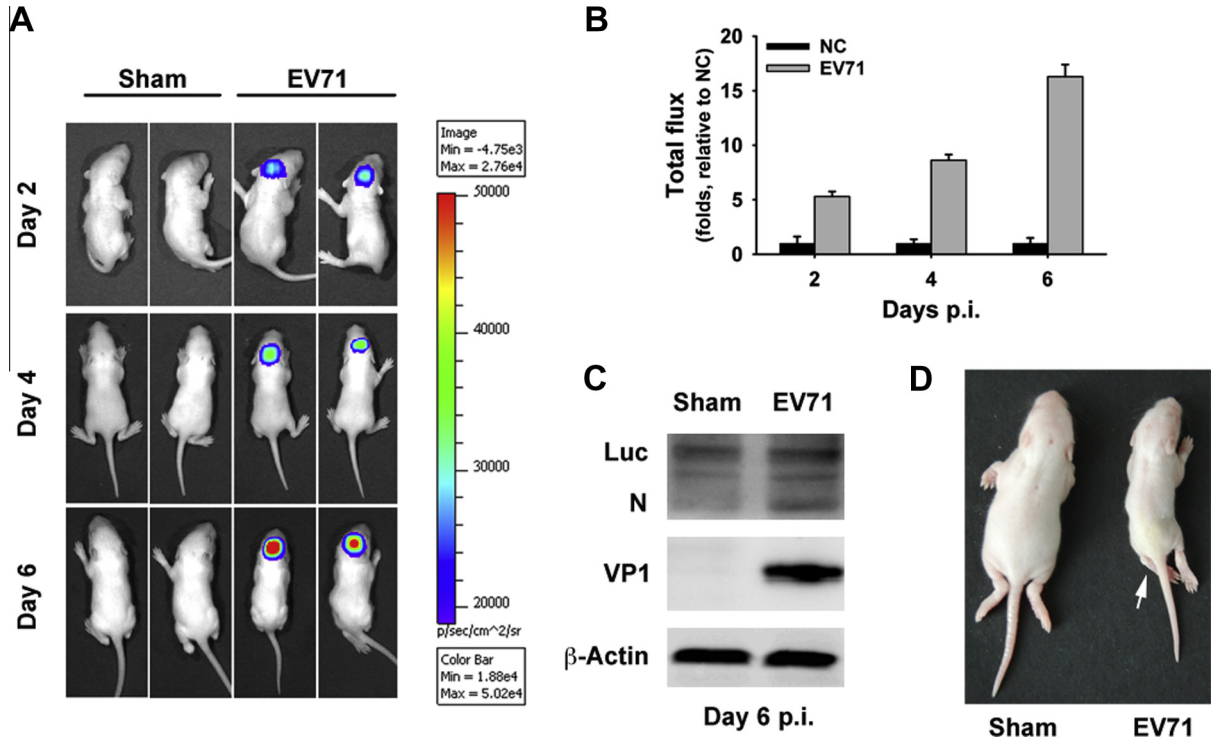

Fig. 3. The bioluminescence imaging of the EV71 infected mice with AmN(Q/G)BC expression. Three-day-old ICR mice were infected with 2×10^7 TCID50 of EV71 by intracerebral injection. The DNA of pAmN(Q/G)BC was intracerebrally inoculated into the mice 24 h before bioluminescence detection. (A and B) The bioluminescence imaging of the mice on day 2, 4, and 6 p.i. The protocol for the sham-treated mice was identical to that for the infected mice except for the use of PBS instead of the virus. The total flux was normalized to that of the sham-treated mice. Error Bars represent SD ($n = 3$). (C) The expression of Luc, N fragment, and VP1 proteins in the mouse brain on day 6 p.i. (D) Symptoms of the EV71-infected mice. The infected mice showed severe body weight loss, hind limb paralysis (arrow), and skin lesions on day 6 p.i.

3.5. AmN(Q/G)BC can visualize the inhibitory effect of GW5074 and U0126 on EV71 infection under in vitro condition in a dose-dependent manner

GW5074 and U0126 were selected to evaluate the application of AmN(Q/G)BC in screening anti-EV71 agents *in vitro*. First, the cytotoxicity of GW5074 and U0126 in Vero cells was tested using the MTT assay. The treatment with GW5074 from 0 to 20 μM or with U0126 from 0 to 60 μM did not significantly affect the cell viability (Fig. S3).

To determine the anti-EV71 effect of GW5074 and U0126, Vero cells were infected with 1.5×10^6 TCID50 of EV71. The culture medium was replaced with the DMEM containing GW5074 (0, 5, and 20 μM), U0126 (0, 20, and 60 μM), and GW5074 + U0126 at 1 h p.i. The CPE and cell viability were observed within 24 h p.i. As shown in Fig. S4A, severe CPE including cell rounding and lysis was observed in the cells without GW5074/U0126 treatment (Sham), while the CPE in the cells treated with GW5074, U0126, or GW5074 + U0126 was significantly inhibited in a dose-dependent manner. GW5074 showed better CPE inhibition than U0126.

The cell viability of the infected cells treated with 5 μM GW5074 was approximately 80% of that of the non-infected cells (NC) at 24 h p.i. (Fig. S4B). It increased to approximately 96% when GW5074 was at a concentration of 20 μM (Fig. S4B). In the infected cells treated with 20 μM U0126, the cell viability was approximately 60% compared with the NC group at 24 h p.i. (Fig. S4C). When treated with 60 μM U0126, the cell viability increased to 80% (Fig. S4C). Interestingly, compared with the GW5074-treated cells, the combination of GW5074 and U0126 did not further increase the cell viability (Fig. S4D), suggesting that GW5074 was more competent than U0126 in terms of the anti-EV71 potential.

To determine the anti-EV71 effect of GW5074 and U0126 with AmN(Q/G)BC reporter, Vero cells in a 24-well plate were transfected with pAmN(Q/G)BC for 24 h. The cells were inoculated with 5×10^6 TCID50 of EV71 and incubated at 37 °C for 1 h for virus attachment. The medium was replaced with DMEM containing GW5074, U0126, and GW5074 + U0126. Luc bioluminescence was detected at 4 h p.i. The cellular proteins were extracted at 7 h p.i. for Western blotting. As shown in Fig. 5, the treatments of GW5074 (5, 10, and 20 μM), U0126 (20, 40, and 60 μM), or GW5074 + U0126 (5 + 20, 10 + 40, and 20 + 60 μM) significantly decreased the photonic fluxes in the infected cells in a dose-dependent manner ($P < 0.01$ except 20 μM U0126, which was $P < 0.05$) (Fig. 4A, C, and E). Western blotting showed that the treatments also decreased the VP1 and N expression in a dose-dependent manner (Fig. 4B–I). The photonic fluxes were reduced to approximately 60% and 40% in the presence of 10 and 20 μM GW5074 compared to the control cells, respectively (Fig. 4A). The treatment with U0126 significantly inhibited the photonic flux but to a lesser degree compared to the treatment with GW5074 (Fig. 4C). The combination of GW5074 and U0126 showed an enhanced inhibition on the photonic fluxes in the infected cells (Fig. 4E). These data were consistent with the CPE and MTT detection.

Furthermore, GW5074 treatment also dose-dependently decreased the levels of phosphorylated Raf-1 (p-Raf), phosphorylated ERK1/2 (p-ERK), and VP1 protein ($P < 0.01$) in the infected cells (Fig. 4G and J). U0126 treatment did not influence the level of p-Raf but decreased the expression of p-ERK as well as VP1 in a dose-dependent manner (Fig. 4H and K). The GW5074 + U0126 combinations were able to block both the p-Raf and p-ERK expression and significantly inhibited the VP1 expression as well ($P < 0.01$) (Fig. 4I and L). Interestingly, the treatment with 2.5 μM

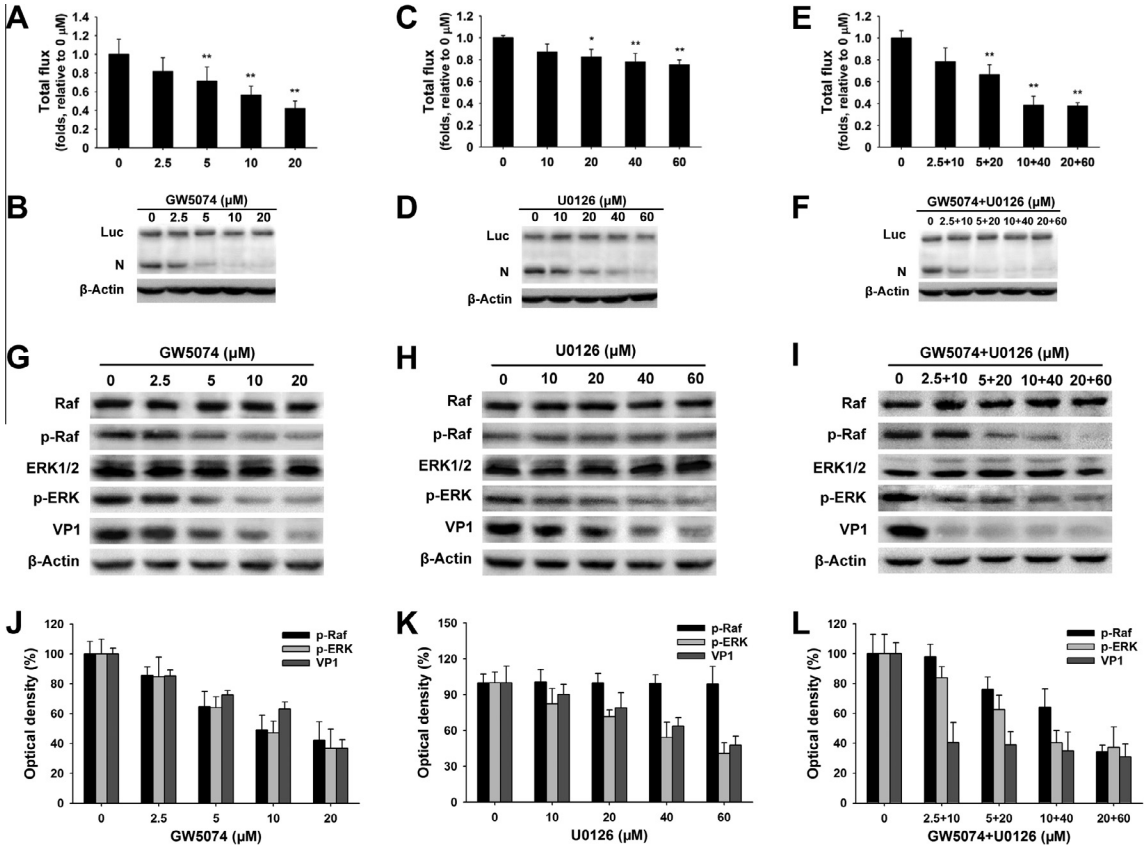

Fig. 4. The *in vitro* antiviral effect of GW5074 and U0126 evaluated by bioluminescence imaging. (A, C, and E) Vero cells grown in 24-well plates were transfected with pAmN(Q/G)BC. The cells were infected with EV71 at 24 h post-transfection. The culture medium was replaced with DMEM containing GW5074, U0126, and GW5074 + U0126 1 h after the virus inoculation, respectively. The bioluminescence was detected at 4 h p.i. with an IVIS Lumina camera. The total fluxes of the treated cells were normalized to that of the cells without treatment (0 μM). Error bars represent SE ($n = 3$). * and ** stands for $P < 0.05$ and $P < 0.01$, respectively, compared with the untreated cells. (B, D, and F) The protein expression of Luc and N fragment in the cells at 7 h p.i. (G–L). The western blotting of Raf-1 (Raf), p-Raf-1 (p-Raf), ERK1/2, p-ERK1/2 (p-ERK), EV71 VP1, and β-actin in the cells treated with GW5074, U0126, and GW5074 + U0126, respectively. The optical density values of the blots (J, K, and L) were normalized to β-actin. Error bars represent SD ($n = 3$). * and ** represent $P < 0.05$ and $P < 0.01$ compared with the untreated cells.

GW5074 or 10 μM U0126 showed only approximately 10% inhibition on the VP1 expression (Fig. 4G and H), while the combination of 2.5 μM GW5074 + 10 μM U0126 inhibited the VP1 expression by approximately 60% (Fig. 4I). The inhibition efficiency of this dose combination almost equaled that of the high dose combinations (Fig. 4I), suggesting that there was a synergistic effect of GW5074 and U0126, probably by double blocking the phosphorylation of MAP kinases.

3.6. AmN(Q/G)BC can monitor the therapeutic effect of anti-EV71 agents in vivo

The *in vivo* toxicity of GW5074 and U0126 was evaluated first. Suckling ICR mice were administered GW5074 (0, 0.05, 0.1, and 0.2 mg/kg), U0126 (0, 0.25, 0.5, and 1.0 mg/kg), and GW5074 + U0126, through intraperitoneal injection. The brain, heart, kidney, liver, and lung tissues were collected and subjected to histopathology examination on day 6 after the administration. We did not observe any apparent body weight difference among various groups. No obvious lesions were found in the mice treated with GW5074 up to 0.2 mg/kg, U0126 up to 1.0 mg/kg, and GW5074 (0.2 mg/kg) + U0126 (1.0 mg/kg) histopathologically (Fig. S5). Therefore, the doses of 0.2 mg/kg GW5074 and 1.0 mg/kg U0126 were chosen for the *in vivo* study.

To monitor the *in vivo* anti-EV71 effect, 3-day-old ICR mice were infected with 2×10^7 TCID50 of EV71 by intracerebral injection. The mice were treated with GW5074 (0.2 mg/kg), U0126 (1.0 mg/kg), and GW5074 (0.2 mg/kg) + U0126 (1.0 mg/kg) through intraperitoneal injection at 24 h p.i. The treatments were repeated twice at an interval of 48 h. pAmN(Q/G)BC (10 μg per mouse) was administered intracerebrally at the same time of the drug administration. Bioluminescence imaging was detected on day 2, 4, and 6 p.i. (Fig. 5A). The mice were sacrificed on day 6 p.i., and the brain tissues were collected for histopathology examination. As shown in Fig. 5B, the photonic flux was not detected in the non-infected normal control (NC) mice, whereas the infected mice showed bioluminescence signal in their heads from day 2 p.i. (Fig. 5C). On day 4 and 6 p.i., the photonic flux remained low in the mice treated with GW5074, U0126, and GW5074 + U0126 (Fig. 5B and C), while it continuously increased in the sham group. We found no significant difference between the photonic fluxes in the mice treated with GW5074 and U0126 ($P > 0.05$).

Symptomatically, the infected mice showed severe hind limb paralysis (Video S2), whereas the mice treated with GW5074 and U0126 only showed mild limb paralysis, especially the mice treated with GW5074 (Video S3–S5). Histopathology observation showed that the granular layers of the cerebral cortex were disrupted in the infected mice (Fig. 6C). In contrast, the brain histological structure was much healthier in the mice treated with GW5074, U0126, or GW5074 + U0126 (Fig. 6E, G, and I). In addition, the majority of the multiform layer neurons in the infected

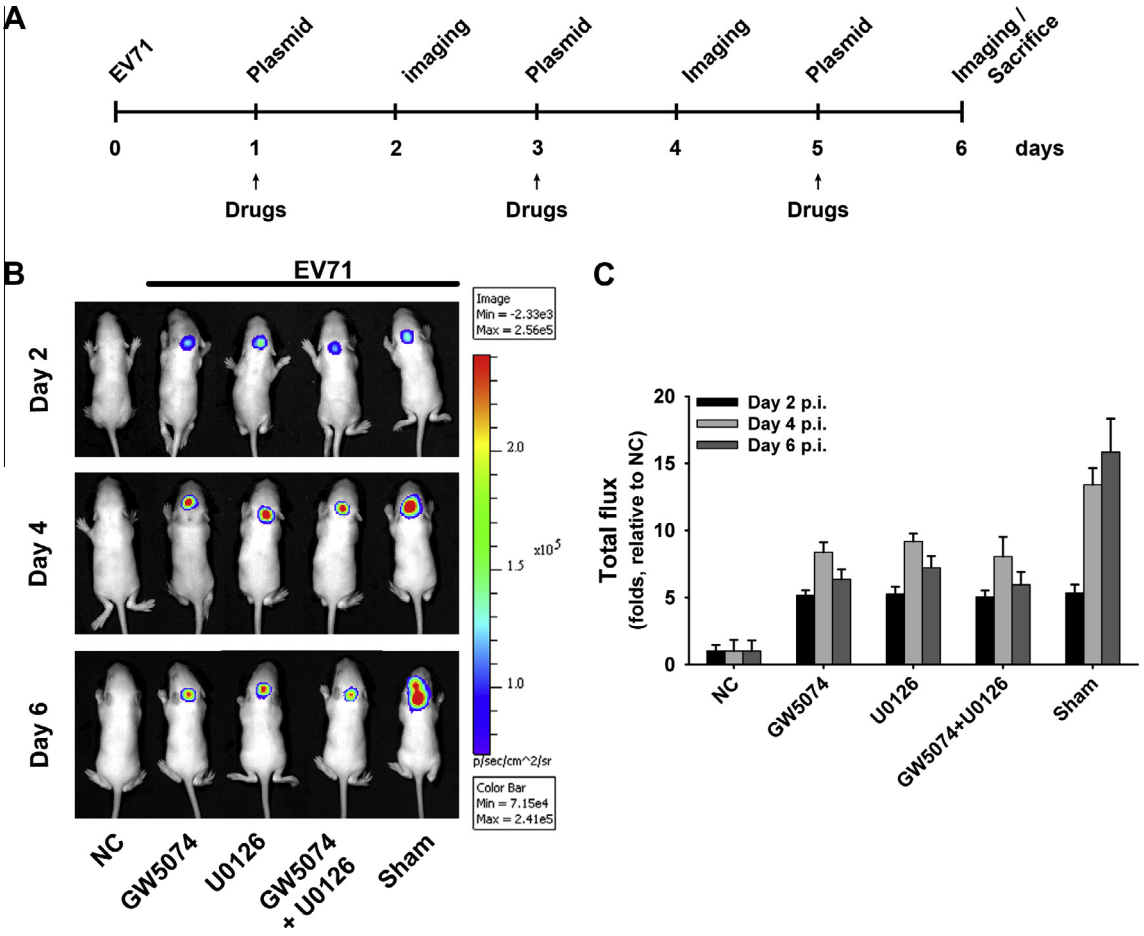

Fig. 5. The *in vivo* antiviral effect of GW5074 and U0126 evaluated by bioluminescence imaging with AmN(Q/G)BC reporter. (A) The protocol of the *in vivo* experiments. Three-day-old ICR mice were infected with EV71 by intracerebral injection. The infected mice were treated with GW5074 (20 μM), U0126 (60 μM), and GW5074 + U0126 (20 μM + 60 μM) 3 times at an interval of 48 h from 24 h p.i. pAmN(Q/G)BC was intracerebrally inoculated into the mice at the time of drug administration. The bioluminescence was detected on day 2, 4, and 6 p.i. (B) The bioluminescence imaging of the mice. Experiments were repeated 3 times, and the representative images are presented. NC: the normal control mice, which were treated as the other groups except inoculating PBS instead of virus. Sham: the infected mice without drug treatment. (C) The total fluxes of the mice normalized to that of the NC mice. Error bars represent SD (n = 3).

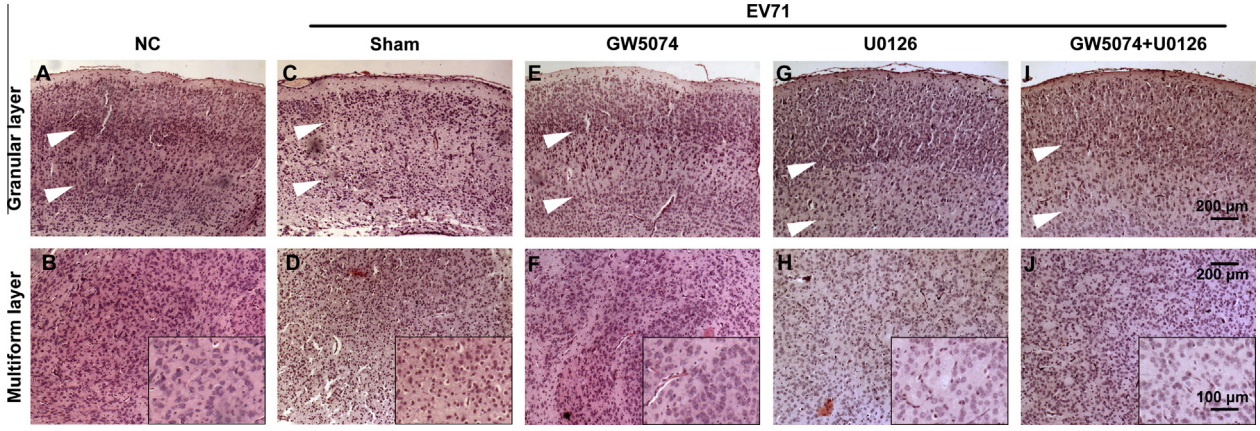

Fig. 6. The *in vivo* antiviral effect of GW5074 and U0126 evaluated by histopathology examination. The brain tissues of the tested mice (Fig. 5) were harvested for histopathology examination. The images of the granular layers and the multiform layer of cerebral cortex are shown separately. The arrow shows the external and internal granular layers (A, C, E, G, and I). The enlarged views of the neurons in the multiform layer are shown in the lower right corner (B, D, F, H, and J). NC: the normal control mice. Sham: the infected mice without drug treatment.

mice were undergoing nucleus shrinkage, a sign of apoptosis-like injury (Fig. 6D). In the treated mice, however, nucleus shrinkage only occurred in a few of the multiform layer neurons (Fig. 6F, H, and J). The bioluminescence imaging was consistent with histopathology evidence, indicating that the AmN(Q/G)BC-based bioluminescence imaging can detect the *in vivo* EV71 infection in a real-time manner. These data also suggest that GW5074 and U0126 can exert their anti-EV71 effect under *in vivo* conditions.

4. Discussion

EV71 infection, the major cause of HFMD, has been one of the critical public health concerns in the past decades worldwide especially in the Asia–Pacific region (Shih et al., 2011; Yan et al., 2012; Zeng et al., 2012b). Effective vaccine and treatment against EV71 are still lacking. The conventional detection methods for EV71 infection are not real-time based. Although fluorescence protein- or luciferase-expressing picornavirus variants can be used to visually monitor the virus infection (Tong et al., 2011; Wang et al., 2012c), the defects such as genome destabilization (Lee et al., 2002; Tong et al., 2011) and phenotype alteration (Lee et al., 2002; Tong et al., 2011) limit its application. Furthermore, these variants are not suitable for *in vivo* observation because of the short emission wavelength.

Protein fragment complementation strategy has been used to study cellular protein interactions, metabolism, and biochemical processes (Ear and Michnick, 2009; Xie et al., 2012). Split luciferase approach requires protease to cleave the splitting Luc molecule and restore its luciferase activity. It is applicable especially to a virus that expresses protease, e.g., hepatitis C virus, which possesses NS3/4A protease (Wang et al., 2010). EV71 expresses a cysteine protease $3C^{pro}$ that plays a key role in viral protein maturation (Cui et al., 2011; Lu et al., 2011; Shih et al., 2011; Zhang et al., 2013). In this study, we adapted the split luciferase imaging strategy to generate an AmN(Q/G)BC reporter for monitoring EV71 infection by response to the presence of $3C^{pro}$. The antiviral effect of GW5074 and U0126 was evaluated using this approach. Our observations demonstrated that this real-time approach could visually and quantitatively detect EV71 infection. The *in vitro* and *in vivo* anti-EV71 effect of GW5074 and U0126 could be efficiently monitored by this approach. Thus, this approach might be useful for high-throughput screening of anti-EV71 agents.

To ensure that the reporter molecule is completely cleaved by EV71 $3C^{pro}$, we designed two consecutive $3C^{pro}$ cleavage sites in the oligopeptide AVMQGASIQG. Both the bioluminescence assay and Western blotting confirmed that this oligopeptide could be efficiently cleaved by the $3C^{pro}$ expressed by pEGFP-3C and EV71, and thereafter, the Luc activity was restored. However, the reporter based on the prototype Luc failed to restore the Luc activity dose-dependently. When high doses of viruses were applied, the photonic flux dramatically dropped to a low level. It seems that the Q–G bonds in the Luc itself might be cleaved by $3C^{pro}$. Luc cleavage in poliovirus-infected cells has been observed previously in Dr. Xiaoyu Li's laboratory (personal communication).

Using Q159M and Q338C mutations, the Luc activity restoration of AmN(Q/G)BC became consistently viral dose-dependent (Fig. 2B, C, and D). The bioluminescence imaging was consistent with the level of N expression both *in vitro* and *in vivo* (Fig. 2–4). The cerebral inoculation of pAmN(Q/G)BC successfully traced the EV71 infection in the brains up to 6 days p.i. (Fig. 3 and S2). The imaging was consistent with the cerebral injury of the infected mice as well (Fig. 6). EV71 replication could be detected using the bioluminescence approach as early as 4 h p.i. *in vitro*, which was much earlier than the CPE. These data indicate that the AmN(Q/G)BC reporter is a reliable biosensor for detecting EV71 infection.

GW5074 and U0126, two MAPK inhibitors, were identified as anti-EV71 agents under *in vitro* conditions (Arita et al., 2008, 2009; Wang et al., 2012a). Picornavirus infection usually activates the MAPK pathway during the attachment and biosynthesis phases (Luo et al., 2002). Conversely, the MAPK activation is necessary for picornavirus replication. Blocking ERK phosphorylation can significantly inhibit the replication of coxsackievirus B3 (Lim et al., 2005a; Luo et al., 2002; Wang et al., 2012a). Inhibition of ERK phosphorylation by U0126 results in a significant decrease in EV71 replication (Lim et al., 2005a; Luo et al., 2002; Wang et al., 2012a). Our results confirmed that either GW5074 or U0126 alone blocks ERK1/2 phosphorylation and inhibits EV71 replication and photonic flux under *in vitro* conditions (Fig. 4 and S4). GW5074 combined with U0126 showed a synergistic inhibitory effect on EV71 replication (Fig. 4 and S4). Therefore, GW5074 and U0126 were employed as anti-EV71 agents in this study to validate the *in vivo* application of AmN(Q/G)BC reporter in terms of anti-EV71 drug evaluation and screening.

In the mice with EV71 cerebral infection, the treatments with GW5074 and/or U0126 significantly decreased the photonic flux (Fig. 5) and the cerebral injury (Fig. 6) as well as the limb paralysis (Video S3 and S5). GW5074 and U0126 therefore efficiently protect mice from the EV71 cerebral infection. The *in vivo* bioluminescence imaging was consistent with the histopathology observation, suggesting that AmN(Q/G)BC can be a "visualizer" for *in vivo* anti-EV71 drug screening.

Our study also demonstrated that the anti-EV71 efficacy of GW5074 was better than that of U0126 (Fig. 4). Recent studies recognized phosphatidylinositol-4-kinase IIIβ (PI4KIIIβ) as a host target of GW5074 (Arita et al., 2011; van der Schaar et al., 2012). PI4KIIIβ and its derivative phosphatidylinositol-4-phosphate (PI4P) are required for enteroviral RNA replication (Hsu et al., 2010). This finding provides a reasonable explanation for the better anti-EV71 efficacy of GW5074. Furthermore, GW5074 is a brain-permeable 3′ substituted indolone, which can inhibit neuronal cell death *in vitro* (Chin et al., 2004). GW5074 has been used for *in vivo* study for a short period and no acute toxicity reported (Chen et al., 2008). We did not observe any obvious abnormality in the GW5074-treated mice within 6 days (Fig. S5). Thus, GW5074 is probably a valuable pharmaceutical compound for clinical chemotherapy against EV71 infection.

Plasmid DNA-based gene therapy has been successfully used for research and for the clinical treatment of central nervous diseases (Shimamura et al., 2011). The accumulated evidence indicates that animal cells within a tissue architecture can directly uptake naked DNA; thus, plasmid DNA can be delivered to cells *in vivo* and lead to gene expression (Herweijer and Wolff, 2003). The reporter developed in this study is plasmid-based. The disadvantage is that the plasmid needs to be inoculated repeatedly to ensure long-term expression. Developing a viral vector-based reporter and transgenic mouse line would be better for high-throughput drug screening. Moreover, this approach may be applicable to other picornaviruses because the $3C^{pro}$ target sequence of EV71 is identical to that of poliovirus and coxsackievirus (Nicklin et al., 1988; Yun et al., 2012).

Acknowledgments

This work was supported by the Natural Science Foundation of China (NSFC) (81271825 to Z. Zhong, 31270198 to W. Zhao, 81101234 to T. Lei, and 81101235 to Y. Wang). The funder had no role in the study design, data collection and analysis, decision to publish, or the preparation of the manuscript. We are grateful to Prof. Mingli Wang, Department of Microbiology, Anhui Medical University, Hefei, China for the kind gift of the EV71 strain. We thank Dr. Xiaoyu Li, Division of Gastroenterology, University of Florida, Jacksonville, FL. for the insightful discussion and Prof. Yong-Chuan Wong, Department of Anatomy, Faculty of Medicine, University of Hong Kong, Hong Kong, for revising the manuscript. We thank Heilongjiang Provincial Key Laboratory of Pathogens and Immunity, and Heilongjiang Provincial Science and Technology Innovation Team in Higher Education Institutes for Infection and Immunity, Harbin Medical University, Harbin 150081, China for their technical support. The Northern Translational Medicine

Research Center of Harbin Medical University also provided technical support for this work.

Appendix A. Supplementary data

Supplementary data associated with this article can be found, in the online version, at http://dx.doi.org/10.1016/j.antiviral.2013.11.002.

References

Arita, M., Kojima, H., Nagano, T., Okabe, T., Wakita, T., Shimizu, H., 2011. Phosphatidylinositol 4-kinase III beta is a target of enviroxime-like compounds for antipoliovirus activity. J. Virol. 85, 2364–2372.

Arita, M., Wakita, T., Shimizu, H., 2008. Characterization of pharmacologically active compounds that inhibit poliovirus and enterovirus 71 infectivity. J. Gen. Virol. 89, 2518–2530.

Arita, M., Wakita, T., Shimizu, H., 2009. Cellular kinase inhibitors that suppress enterovirus replication have a conserved target in viral protein 3A similar to that of enviroxime. J. Gen. Virol. 90, 1869–1879.

Au, J.T., Gonzalez, L., Chen, C.H., Serganova, I., Fong, Y., 2012. Bioluminescence imaging serves as a dynamic marker for guiding and assessing thermal treatment of cancer in a preclinical model. Ann. Surg. Oncol. 19, 3116–3122.

Bain, J., Plater, L., Elliott, M., Shpiro, N., Hastie, C.J., McLauchlan, H., Klevernic, I., Arthur, J.S., Alessi, D.R., Cohen, P., 2007. The selectivity of protein kinase inhibitors: a further update. Biochem. J. 408, 297–315.

Brock, M., 2012. Application of bioluminescence imaging for in vivo monitoring of fungal infections. Int. J. Microbiol. 2012, 956794.

Chang, J.Y., Chang, C.P., Tsai, H.H., Lee, C.D., Lian, W.C., Ih Jen, S., Sai, I.H., Liu, C.C., Chou, A.H., Lu, Y.J., Chen, C.Y., Lee, P.H., Chiang, J.R., Chong, P.C., 2012. Selection and characterization of vaccine strain for enterovirus 71 vaccine development. Vaccine 30, 703–711.

Chen, H.M., Wang, L., D'Mello, S.R., 2008. Inhibition of ATF-3 expression by B-Raf mediates the neuroprotective action of GW5074. J. Neurochem. 105, 1300–1312.

Chen, Y.C., Yu, C.K., Wang, Y.F., Liu, C.C., Su, I.J., Lei, H.Y., 2004. A murine oral enterovirus 71 infection model with central nervous system involvement. J. Gen. Virol. 85, 69–77.

Chin, P.C., Liu, L., Morrison, B.E., Siddiq, A., Ratan, R.R., Bottiglieri, T., D'Mello, S.R., 2004. The c-Raf inhibitor GW5074 provides neuroprotection in vitro and in an animal model of neurodegeneration through a MEK-ERK and Akt-independent mechanism. J. Neurochem. 90, 595–608.

Cui, S., Wang, J., Fan, T., Qin, B., Guo, L., Lei, X., Wang, M., Jin, Q., 2011. Crystal structure of human enterovirus 71 3C protease. J. Mol. Biol. 408, 449–461.

Deng, J.X., Nie, X.J., Lei, Y.F., Ma, C.F., Xu, D.L., Li, B., Xu, Z.K., Zhang, G.C., 2012. The highly conserved 5' untranslated region as an effective target towards the inhibition of enterovirus 71 replication by unmodified and appropriate 2′-modified siRNAs. J. Biomed. Sci. 19, 73.

Doyle, T.C., Burns, S.M., Contag, C.H., 2004. In vivo bioluminescence imaging for integrated studies of infection. Cell. Microbiol. 6, 303–317.

Du, J., Zhao, F., Zhou, Y., Yan, H., Duan, X.G., Liang, S.Q., Wang, Y.L., Fu, Q.X., Wang, X.H., Peng, J.C., Zhan, L.S., 2010. Bioluminescence imaging allows monitoring hepatitis C virus core protein inhibitors in mice. PLoS One 5, e14043.

Ear, P.H., Michnick, S.W., 2009. A general life-death selection strategy for dissecting protein functions. Nat. Methods 6, 813–816.

Geiss, B.J., Stahla-Beek, H.J., Hannah, A.M., Gari, H.H., Henderson, B.R., Saeedi, B.J., Keenan, S.M., 2011. A high-throughput screening assay for the identification of flavivirus NS5 capping enzyme GTP-binding inhibitors: implications for antiviral drug development. J. Biomol. Screen. 16, 852–861.

Heaton, N.S., Leyva-Grado, V.H., Tan, G.S., Eggink, D., Hai, R., Palese, P., 2013. In vivo bioluminescent imaging of influenza A virus infection and characterization of novel cross-protective monoclonal antibodies. J. Virol.. http://dx.doi.org/10.1128/JVI.00969-13.

Herweijer, H., Wolff, J.A., 2003. Progress and prospects: naked DNA gene transfer and therapy. Gene Ther. 10, 453–458.

Hsu, N.Y., Ilnytska, O., Belov, G., Santiana, M., Chen, Y.H., Takvorian, P.M., Pau, C., van der Schaar, H., Kaushik-Basu, N., Balla, T., Cameron, C.E., Ehrenfeld, E., van Kuppeveld, F.J., Altan-Bonnet, N., 2010. Viral reorganization of the secretory pathway generates distinct organelles for RNA replication. Cell 141, 799–811.

Johnson, G.L., Lapadat, R., 2002. Mitogen-activated protein kinase pathways mediated by ERK, JNK, and p38 protein kinases. Science 298, 1911–1912.

Khong, W.X., Foo, D.G., Trasti, S.L., Tan, E.L., Alonso, S., 2011. Sustained high levels of interleukin-6 contribute to the pathogenesis of enterovirus 71 in a neonate mouse model. J. Virol. 85, 3067–3076.

Krah, D.L., 1991. A simplified multiwell plate assay for the measurement of hepatitis A virus infectivity. Biologicals 19, 223–227.

Lee, S.G., Kim, D.Y., Hyun, B.H., Bae, Y.S., 2002. Novel design architecture for genetic stability of recombinant poliovirus: the manipulation of G/C contents and their distribution patterns increases the genetic stability of inserts in a poliovirus-based RPS-Vax vector system. J. Virol. 76, 1649–1662.

Li, J., Huo, X., Dai, Y., Yang, Z., Lei, Y., Jiang, Y., Li, G., Zhan, J., Zhan, F., 2012a. Evidences for intertypic and intratypic recombinant events in EV71 of hand, foot and mouth disease during an epidemic in Hubei Province, China, 2011. Virus Res. 169, 195–202.

Li, Y.P., Liang, Z.L., Gao, Q., Huang, L.R., Mao, Q.Y., Wen, S.Q., Liu, Y., Yin, W.D., Li, R.C., Wang, J.Z., 2012b. Safety and immunogenicity of a novel human enterovirus 71 (EV71) vaccine: a randomized, placebo-controlled, double-blind, Phase I clinical trial. Vaccine 30, 3295–3303.

Lim, B.K., Nam, J.H., Gil, C.O., Yun, S.H., Choi, J.H., Kim, D.K., Jeon, E.S., 2005a. Coxsackievirus B3 replication is related to activation of the late extracellular signal-regulated kinase (ERK) signal. Virus Res. 113, 153–157.

Lim, B.K., Shin, J.O., Lee, S.C., Kim, D.K., Choi, D.J., Choe, S.C., Knowlton, K.U., Jeon, E.S., 2005b. Long-term cardiac gene expression using a coxsackieviral vector. J. Mol. Cell. Cardiol. 38, 745–751.

Liu, C.C., Lian, W.C., Butler, M., Wu, S.C., 2007. High immunogenic enterovirus 71 strain and its production using serum-free microcarrier Vero cell culture. Vaccine 25, 19–24.

Lu, G., Qi, J., Chen, Z., Xu, X., Gao, F., Lin, D., Qian, W., Liu, H., Jiang, H., Yan, J., Gao, G.F., 2011. Enterovirus 71 and coxsackievirus A16 3C proteases: binding to rupintrivir and their substrates and anti-hand, foot, and mouth disease virus drug design. J. Virol. 85, 10319–10331.

Luo, H., Yanagawa, B., Zhang, J., Luo, Z., Zhang, M., Esfandiarei, M., Carthy, C., Wilson, J.E., Yang, D., McManus, B.M., 2002. Coxsackievirus B3 replication is reduced by inhibition of the extracellular signal-regulated kinase (ERK) signaling pathway. J. Virol. 76, 3365–3373.

Madero-Visbal, R.A., Colon, J.F., Hernandez, I.C., Limaye, A., Smith, J., Lee, C.M., Arlen, P.A., Herrera, L., Baker, C.H., 2012. Bioluminescence imaging correlates with tumor progression in an orthotopic mouse model of lung cancer. Surg. Oncol. 21, 23–29.

Nicklin, M.J., Harris, K.S., Pallai, P.V., Wimmer, E., 1988. Poliovirus proteinase 3C: large-scale expression, purification, and specific cleavage activity on natural and synthetic substrates in vitro. J. Virol. 62, 4586–4593.

Pourianfar, H.R., Poh, C.L., Fecondo, J., Grollo, L., 2012. In vitro evaluation of the antiviral activity of heparan sulfate mimetic compounds against enterovirus 71. Virus Res. 169, 22–29.

Sewald, X., Gonzalez, D.G., Haberman, A.M., Mothes, W., 2012. In vivo imaging of virological synapses. Nat. Commun. 3, 1320.

Shang, B., Deng, C., Ye, H., Xu, W., Yuan, Z., Shi, P.Y., Zhang, B., 2012a. Development and characterization of a stable eGFP enterovirus 71 for antiviral screening. Antiviral. Res. 97, 198–205.

Shang, L., Xu, M., Yin, Z., 2012b. Antiviral drug discovery for the treatment of enterovirus 71 infections. Antiviral. Res. 97, 183–194.

Shekhawat, S.S., Ghosh, I., 2011. Split-protein systems: beyond binary protein-protein interactions. Curr. Opin. Chem. Biol. 15, 789–797.

Shih, S.R., Stollar, V., Li, M.L., 2011. Host factors in enterovirus 71 replication. J. Virol. 85, 9658–9666.

Shimamura, M., Sato, N., Morishita, R., 2011. Experimental and clinical application of plasmid DNA in the field of central nervous diseases. Curr. Gene Ther. 11, 491–500.

Shimizu, S., 2004. Routs of administration. In: Hedrich, H.J., Bullock, G. (Eds.), The Laboratory Mouse. Elsevier Academic Press, Landon, UK, pp. 527–541.

Snoeks, T.J., van Beek, E., Que, I., Kaijzel, E.L., Lowik, C.W., 2012. Bioluminescence imaging of bone metastasis in rodents. Methods Mol. Biol. 816, 507–515.

Tan, E.L., Tan, T.M., Tak Kwong Chow, V., Poh, C.L., 2007. Inhibition of enterovirus 71 in virus-infected mice by RNA interference. Mol. Ther. 15, 1931–1938.

Thormeyer, D., Ammerpohl, O., Larsson, O., Xu, Y., Asinger, A., Wahlestedt, C., Liang, Z., 2003. Characterization of lacZ complementation deletions using membrane receptor dimerization. Biotechniques 34 (346–350), 345–352.

Tong, L., Lin, L., Zhao, W., Wang, B., Wu, S., Liu, H., Zhong, X., Cui, Y., Gu, H., Zhang, F., Zhong, Z., 2011. Destabilization of coxsackievirus b3 genome integrated with enhanced green fluorescent protein gene. Intervirology 54, 268–275.

van der Schaar, H.M., van der Linden, L., Lanke, K.H., Strating, J.R., Purstinger, G., de Vries, E., de Haan, C.A., Neyts, J., van Kuppeveld, F.J., 2012. Coxsackievirus mutants that can bypass host factor PI4KIIIbeta and the need for high levels of PI4P lipids for replication. Cell Res. 22, 1576–1592.

Wang, B., Zhang, H., Zhu, M., Luo, Z., Peng, Y., 2012a. MEK1-ERKs signal cascade is required for the replication of enterovirus 71 (EV71). Antiviral. Res. 93, 110–117.

Wang, C.Y., Huang, S.C., Zhang, Y., Lai, Z.R., Kung, S.H., Chang, Y.S., Lin, C.W., 2012b. Antiviral Ability of *Kalanchoe gracilis* leaf extract against enterovirus 71 and coxsackievirus A16. Evid. Based Complement. Alternat. Med. 2012, 503165.

Wang, L., Fu, Q., Dong, Y., Zhou, Y., Jia, S., Du, J., Zhao, F., Wang, Y., Wang, X., Peng, J., Yang, S., Zhan, L., 2010. Bioluminescence imaging of hepatitis C virus NS3/4A serine protease activity in cells and living animals. Antiviral. Res. 87, 50–56.

Wang, L., Qin, Y., Tong, L., Wu, S., Wang, Q., Jiao, Q., Guo, Z., Lin, L., Wang, R., Zhao, W., Zhong, Z., 2012c. MiR-342-5p suppresses coxsackievirus B3 biosynthesis by targeting the 2C-coding region. Antiviral. Res. 93, 270–279.

Weng, K.F., Li, M.L., Hung, C.T., Shih, S.R., 2009. Enterovirus 71 3C protease cleaves a novel target CstF-64 and inhibits cellular polyadenylation. PLoS Pathog. 5, e1000593.

Wu, Z., Yang, F., Zhao, R., Zhao, L., Guo, D., Jin, Q., 2009. Identification of small interfering RNAs which inhibit the replication of several enterovirus 71 strains in China. J. Virol. Methods 159, 233–238.

Xie, W., Pao, C., Graham, T., Dul, E., Lu, Q., Sweitzer, T.D., Ames, R.S., Li, H., 2012. Development of a cell-based high throughput luciferase enzyme fragment complementation assay to identify nuclear-factor-e2-related transcription factor 2 activators. Assay Drug Dev. Technol. 10, 514–524.

Xu, J., Qian, Y., Wang, S., Serrano, J.M., Li, W., Huang, Z., Lu, S., 2010. EV71: an emerging infectious disease vaccine target in the Far East? Vaccine 28, 3516–3521.

Xu, W., Liu, C.F., Yan, L., Li, J.J., Wang, L.J., Qi, Y., Cheng, R.B., Xiong, X.Y., 2012. Distribution of enteroviruses in hospitalized children with hand, foot and mouth disease and relationship between pathogens and nervous system complications. Virol. J. 9, 8.

Yan, X.F., Gao, S., Xia, J.F., Ye, R., Yu, H., Long, J.E., 2012. Epidemic characteristics of hand, foot, and mouth disease in Shanghai from 2009 to 2010: enterovirus 71 subgenotype C4 as the primary causative agent and a high incidence of mixed infections with coxsackievirus A16. Scand. J. Infect. Dis. 44, 297–305.

Yang, Y., Xiu, J., Zhang, X., Zhang, L., Yan, K., Qin, C., Liu, J., 2012a. Antiviral effect of matrine against human enterovirus 71. Molecules 17, 10370–10376.

Yang, Y., Zhang, L., Fan, X., Qin, C., Liu, J., 2012b. Antiviral effect of geraniin on human enterovirus 71 in vitro and in vivo. Bioorg. Med. Chem. Lett. 22, 2209–2211.

Yu, C.K., Chen, C.C., Chen, C.L., Wang, J.R., Liu, C.C., Yan, J.J., Su, I.J., 2000. Neutralizing antibody provided protection against Enterovirus type 71 lethal challenge in neonatal mice. J. Biomed. Sci. 7, 523–528.

Yun, S.H., Lee, W.G., Kim, Y.C., Ju, E.S., Lim, B.K., Choi, J.O., Kim, D.K., Jeon, E.S., 2012. Antiviral activity of coxsackievirus B3 3C protease inhibitor in experimental murine myocarditis. J. Infect. Dis. 205, 491–497.

Zeng, H., Wen, F., Gan, Y., Huang, W., 2012a. MRI and associated clinical characteristics of EV71-induced brainstem encephalitis in children with hand-foot-mouth disease. Neuroradiology 54, 623–630.

Zeng, M., El Khatib, N.F., Tu, S., Ren, P., Xu, S., Zhu, Q., Mo, X., Pu, D., Wang, X., Altmeyer, R., 2012b. Seroepidemiology of enterovirus 71 infection prior to the 2011 season in children in Shanghai. J. Clin. Virol. 53, 285–289.

Zhang, X., Song, Z., Qin, B., Chen, L., Hu, Y., Yuan, Z., 2013. Rupintrivir is a promising candidate for treating severe cases of enterovirus-71 infection: evaluation of antiviral efficacy in a murine infection model. Antiviral. Res. 97, 264–269.

Zhu, F.C., Liang, Z.L., Li, X.L., Ge, H.M., Meng, F.Y., Mao, Q.Y., Zhang, Y.T., Hu, Y.M., Zhang, Z.Y., Li, J.X., Gao, F., Chen, Q.H., Zhu, Q.Y., Chu, K., Wu, X., Yao, X., Guo, H.J., Chen, X.Q., Liu, P., Dong, Y.Y., Li, F.X., Shen, X.L., Wang, J.Z., 2013. Immunogenicity and safety of an enterovirus 71 vaccine in healthy Chinese children and infants: a randomised, double-blind, placebo-controlled phase 2 clinical trial. Lancet 381, 1037–1045.